Stable Flexible Transparent Electrodes for Localized Heating of Lab-on-a-Chip Devices

Dorina Papanastasiou, Abderrahime Sekkat, Viet Huong Nguyen, Carmen Jiménez, David Muñoz-Rojas, Franz Bruckert, Daniel Bellet

Stable flexible transparent electrodes for localized heating of lab-on-a-chip devices

Dorina T. Papanastasiou, Abderrahime Sekkat, Viet H. Nguyen, Carmen Jiménez, David Muñoz-Rojas, Franz Bruckert, Daniel Bellet**

Dr. D.T. Papanastasiou, Dr. A. Sekkat, Dr. C. Jiménez, Dr. D. Muñoz-Rojas, Pr. D. Bellet

Univ. Grenoble Alpes, CNRS, Grenoble INP, LMGP, F- 38016 Grenoble, France

email: franz.bruckert@grenoble-inp.fr, daniel.bellet@grenoble-inp.fr

Dr. V. H. Nguyen

Univ. Grenoble Alpes, CNRS, Grenoble INP, LMGP, F- 38016 Grenoble, France

Faculty of Materials Science and Engineering, Phenikaa University, Hanoi 12116, Viet Nam

Keywords: transparent heaters, spatial atomic layer deposition, microfluidics, chip, selective heating, in situ, DNA

Abstract

In situ biological observations require stable, accurate and local temperature control of specimen. Several heating elements are coupled with microfluidic systems, but few of them are transparent to visible light and therefore compatible with microscopic observation. Traditional transparent electrodes such as indium tin oxide, still suffer from high fabrication cost and brittleness, which is not fully compatible to emerging microfluidic devices. Here, we propose a lightweight, low-cost, flexible transparent heater based on percolating silver nanowire networks, protected with a transparent zinc oxide film, for the *in situ* monitoring of biological experiments. Using the fluorescence of dyes bound to double-stranded DNA to monitor its temperature *in situ*, we demonstrate that such nanocomposites allow rapid and reproducible heating under low applied voltage. Furthermore, selective heating is achieved in different zones of the same microchannel or for adjacent microchannels of the chip heating at different temperatures, with a single transparent heater and bias.

1. Introduction

In situ microscopic observations of biological samples are often conducted in bulky environmental chambers to maintain the proper environment of the cells (temperature, oxygen, pH). Alternatively, several small size heating elements have been developed for lab-on-a-chip devices, but many of them are either complicated or difficult to be mounted, some could have potential water leaks or are not transparent.[1–4] Temperatures of interest range from 30-42 °C for most cell cultures, to 50-95 °C cycles for DNA amplification by Polymerase Chain Reaction (PCR).[3] A few transparent heaters (TH) compatible with biological microscopy observations have been presented in the literature. These studies report the design of PCR microfluidic chips using indium tin oxide (ITO) or graphene as heating elements.[5–7] However, they did not monitor the temperature *in situ* and they do not offer localized and selective heating. In addition, ITO, which is so far the most commonly used transparent conductive material, apart from the limitations based on the indium scarcity and fabrication cost, is challenging to integrate and reuse into microfluidic devices due to its brittleness. Among alternative transparent electrodes investigated in the last decade, silver nanowire (AgNW) networks are one of the most promising emerging technologies.[8–12] Combining low-cost, solution-based fabrication, flexibility, transparency, and high heating performances at low voltage supply, AgNW networks offer a clear asset for integration in TH applications.[13–15] However, bare AgNW networks exhibit degradation of their properties with time or under thermal or electrical stress[16–18]. This can be counteracted by covering them with a thin protective layer of metal oxide; the resulting composite electrode shows excellent electrical stability and durability.[19–21] To the best of our knowledge, TH based on AgNW had not yet been coupled to microfluidic chips, for the *in situ* monitoring of biological observations.

Here we propose a lightweight, and up-scalable TH based on AgNW networks that can easily be integrated into a lab-on-a-chip in an optical microscope. We make use of the well-known denaturation-renaturation cycles of double-stranded DNA (dsDNA) to monitor the fluid temperature *in situ* using SYBR Green I fluorescence. We demonstrate the stable and reproducible heating performance of the TH by encapsulating the AgNW network with thin, protective zinc oxide (ZnO) layer using an open-air scalable ALD approach, namely, atmospheric-pressure spatial atomic layer deposition (AP-SALD), at rather low-temperature ($\leq$ 200 °C).[22–25] The electrical resistance of such AgNW/ZnO nanocomposite remains the same (10-15 Ω) after several bending cycles or hours of electrical or thermal stress. Following the appropriate calibration of the devices (based on the temperature measurements at several points

of the setup), the temperature inside the chip channels can be accurately controlled by supplying a low voltage (<6.5 V) to drive the denaturation-renaturation processes. Furthermore, we demonstrate that the localized heating of the lab-on-a-chip (i.e. heating of different sections of a microchannel or of adjacent channels in a chip at different temperatures) is possible using a single TH element and power source unit. In the present work, we used 3D-printed masks on top of the AgNW networks, during spray-coating deposition, to create specific regions of different network densities and thus local electrical resistivity. This constitutes a low-cost and versatile approach that is compatible to scalable screen-printing techniques,[26,27] and excludes lithography, or other cleanroom patterning processes,[28–30] or other more complex strategies like laser-induced local heating.[31]

2. Results & Discussion

2.1 Fabrication and integration of Transparent Heaters into lab-on-a-chip device

AgNW based flexible TH, encapsulated by a protective oxide thin coating, were fabricated by scalable open-air and low-temperature processes, as schematically represented in **Figure 1**a. First, AgNWs (Figure 1b) were deposited on glass or polymer substrates using a homebuilt pneumatic spray system, with the targeted electrical resistance of 10-15 Ω/sq and optical transparency of ~85% (including substrate contribution).[32] In terms of the amount of silver and considering the dimensions of the nanowires used in the present work, these properties correspond to a network areal mass density (*amd*) of 70±5 mg/m^2.[23] AgNW networks were then coated with thin ZnO films deposited by AP-SALD.[33] The thickness of ZnO was fixed at 30±5 nm to ensure electrode stability (see previous reports and below for more details).[16,21] The temperature and duration of ZnO deposition (200°C for less than 1.5 min) are compatible with the corresponding values of time-of-failure, as reported by Resende et al.,[32] and respect the stability of the AgNW network. Other recently published studies confirm that thermally-sensitive materials are not affected by the oxide deposition by spatial ALD techniques, thanks to their short processing times.[34] Finally, silver paste contacts were applied on the two opposite sides of the AgNW/ZnO specimen and copper wires (2 mm in diameter) were bonded to the silver paste to connect the TH to the power supply. The fabrication process is compatible with roll-to-roll (R2R) and other high throughput in-line processes, i.e. sheet-to-sheet. The reproducibility can be statistically demonstrated on the optical properties of up to 130 spray-

deposited networks, showing a standard deviation of ±1.1% for the total transmittance (Figure S1a).

TEM imaging of bare AgNWs is reported in Figure 1b, while Figure 1c demonstrates the conformal ZnO coating around the AgNWs. At lower magnification, SEM imaging (Figure 1d) exhibits the random distribution of the network. The final TH can be glued to the microfluidic chip using double-sided tape allowing stable bonding with the entire device, as shown in Figure 1e. The lab-on-a-chip can then be placed on the stage of an optical microscope, as presented in Figure 1f. Thanks to the tape, the TH can be easily removed from the chip and reused later, as needed. The IR image shown in Figure 1f reveals the heat generated by the TH upon applying a voltage across the AgNW network. Additional pictures and video of the lab-on-a-chip fabrication steps and integration to the microscope set-up can be found in Figure S2. The fluorescence of the SYBR Green I dye bound to the dsDNA in the solution filling the chip channels could be recorded *in situ* while the TH was heating (i.e. subjected to a voltage). The dye can be excited with blue light ($\lambda_{max} = 497\ nm$) and emits green light ($\lambda_{max} = 520\ nm$). Figure 1g presents an example of the evolution of the recorded fluorescence during heating with a voltage ramp (1 V/min) up to 4.5 V, as well as the extrapolated temperature inside the channel. SYBR Green I exhibits an exceptional affinity for DNA that results in a large fluorescence enhancement upon DNA binding.[35] The dye binds to the minor groove of dsDNA and does not bind to single-stranded DNA (ssDNA). Therefore, a sudden drop in fluorescent signal during the ramp can thus be associated with the DNA melting inside the chip, occurring at 80-81°C. Therefore, thanks to AgNW/ZnO based transparent heater, by applying only few volts, we can reach the DNA denaturation and observe it *in situ*. Following this principle, we performed several experiments that are discussed in the present article.

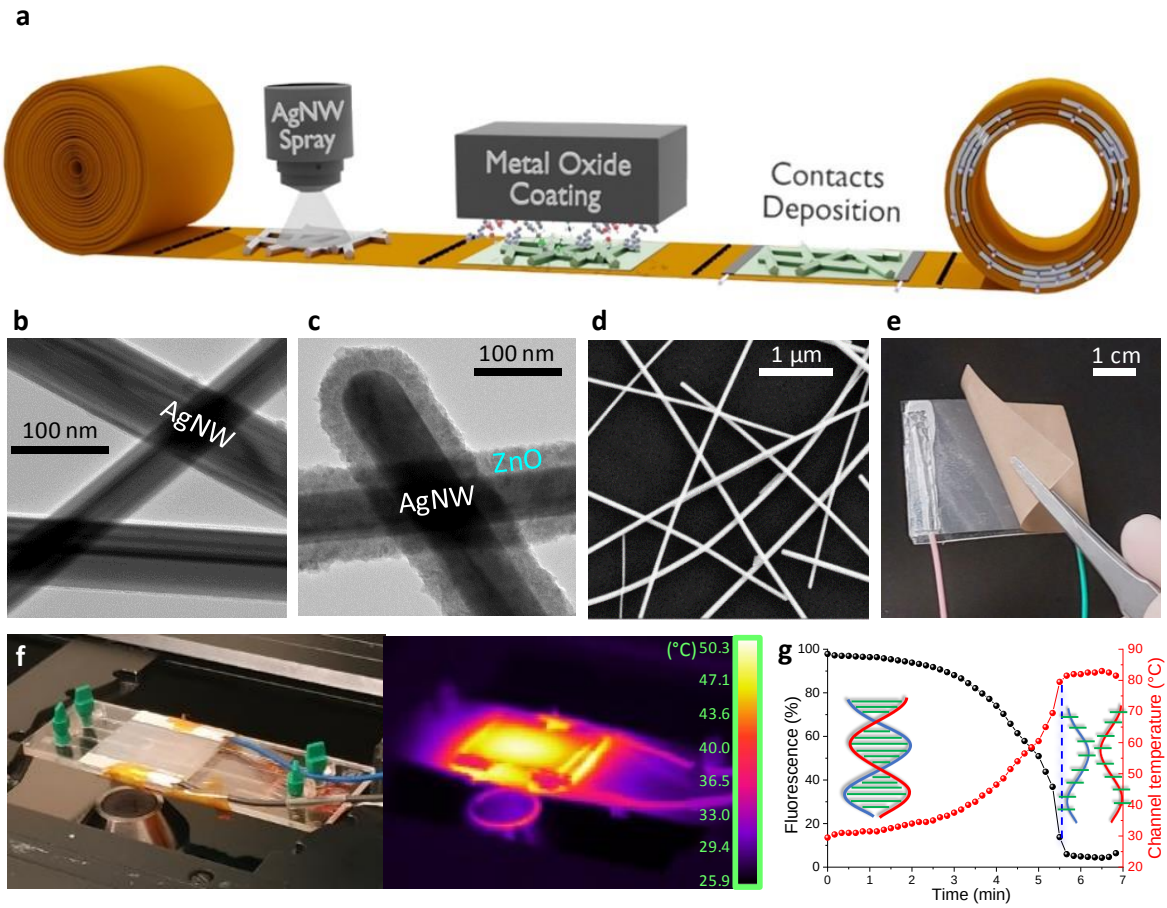

Figure 1. Fabrication of Transparent Heaters and integration into a microfluidic chip to realize a lab-on-a-chip for *in situ* fluorescence measurements. (a) Schematic representation of the fabrication of transparent heaters on flexible substrate, indicating its compatibility with roll-to-roll processes. First, silver nanowires (AgNW) in suspension are deposited by spray coating and then AgNWs are coated by a thin zinc oxide (ZnO) coating by open-air spatial atomic layer deposition. Finally, metallic contacts are deposited to supply the electric bias. (b) Transmission electron microscopy (TEM) image of bare AgNWs. (c) TEM image showing the conformal ZnO coating on the AgNW. The thickness of the coating is about 35 nm. (d) Scanning electron microscopy (SEM) image of a AgNW/ZnO network. (e) AgNW/ZnO based transparent heater (TH) with wires for the electrical connection, and one side stuck on a double-sided adhesive tape. By removing the protective light brown film of the tape, the TH is ready to be stuck to a chip. (f) Optical and infrared (IR) pictures of the lab-on-a-chip fabricated, placed on the stage of an optical microscope. By applying a low voltage, the TH heats the dsDNA in solution inside the chip microchannels. The fluorescence of the SYBR Green I dye, bound to the dsDNA, is recorded *in situ* during the heating. (g) Evolution of fluorescence (in black) during a voltage ramp up to 4.5 V and the extrapolated temperature (in red) inside the channel. The drastic drop

of the fluorescence occurs when the dsDNA reaches its melting point (dashed blue line). As shown in the inset schema, the separation of the DNA strands during denaturation results in an abrupt loss of fluorescence from the dye.

2.2 AgNW/ZnO based TH: properties, stability and reproducibility

Figure 2a exhibits the total transmittance of AgNW/ZnO network compared to bare AgNW network, including the glass substrate contribution (i.e. without any substrate correction). Glass transmittance is plotted as well for reference. The inset picture presents a typical AgNW/ZnO TH specimen with silver paste electrodes. In the visible range (380-750 nm), there is a slight decrease of the average transmittance from 82.0% to 80.1% due to the absorption/reflection of the metal oxide coating (originated from plasmonic absorption). A slight increase was observed for diffuse transmittance, from 5.5% to 6.2% while adding the ZnO coating (Figure S1b). This increase can be explained by more diffuse scattering, this is associated with the light scattering of the nanocomposite interfaces.[36] Having a low fraction of diffuse transmission is essential for the intended application since the larger the diffuse transmittance fraction, the hazier the transparent heater, hindering somehow clear observations. In the NIR range (750-2500 nm), there is also a slight influence of the ZnO coating, the average values of total transmittance are (77.7±3.5)% and (76.8±3.7)% for bare and coated networks, respectively, while the diffuse transmittance in NIR is (5.2±0.3)% and (5.6±0.3)%, respectively. These TH are therefore fully compatible with microscope observations under transmitted illumination, i.e. phase-contrast microscopy. Figure 2b demonstrates the good electro-mechanical properties of the transparent heaters compared to ITO on PEN, commercially purchased from Sigma Aldrich, with an initial sheet resistance of 55 Ω and film thickness of 300 nm. Both bare AgNW and AgNW/ZnO networks show a very stable electrical resistance during 10000 bending cycles of 5 mm radius, in the set-up shown in the inset of Figure 2b, while the ITO loses its high conductivity directly after the first bending cycle.

The TH was subjected to 20 cycles of heating-cooling to investigate its stability, both for bare and coated AgNW networks, between 50 and 120 °C with a ramp rate of ±5 °C/min. As shown in Figure 2c, the ZnO coated networks showed very stable electrical behaviour during 9 hours of measurement, conversely to the bare AgNW networks, which already started degrading after the second heating cycle. The resistance of the nanocomposites followed linearly the evolution of the temperature and the final value after the 20 cycles was almost the same as the initial one

(increase of 0.65%) i.e. no network degradation took place. Furthermore, as reported in SI, the stability of AgNW/ZnO based TH were evaluated also by 20 cycles of electrical stress with a ramp of ±0.5 V/min between 4 and 9 volts. The influence of the ZnO thickness in terms of electrical stability during 20 voltage cycles is reported in the Figure S1c. Between the 10-100 nm range tested, the most stable was the 35 nm and thus it was fixed as optimum oxide thickness value for the rest of the experiments involving the fabricated lab-on-a-chip presented here. The fact that the optimal ZnO thickness appears to be 35 nm is slightly counterintuitive since one could think that thicker coating could correspond to enhanced stability. However several explanations can be proposed, and the prevailing one is the difference of thermal dilation between the ZnO layer and the substrate which can induce structural defects in the layer and leading to a weaker protection. A larger number of cracks in the ZnO layer can exist for thicker ZnO coating.

Finally, the temperature of the sample was recorded during the voltage cycles by using a Pt100 thermocouple, to assess the generated Joule heating. Figure 2d, presents the temperature during the 20 cycles, with a ramp rate of ±0.5 V/min, along with the maximum value of relative change of resistance in each cycle, for AgNW/ZnO TH with an initial resistance of 12.7 Ω. The voltage is varied between 4 and 9 V, which corresponds to a Joule heating of 70 and 140 °C, respectively. It is important to note that these values were intentionally chosen as much higher than the ones needed for the biological samples, in order to ensure a high durability of the THs. Both the electrical resistance and the heating performance of the TH are very reproducible over 7 hours of applied electrical bias. In addition, during the present study, the AgNW/ZnO specimens were used several times, i.e. 48 different biological experiments were carried out in more than 6 months testing the same TH and the latter showed no electrical degradation.

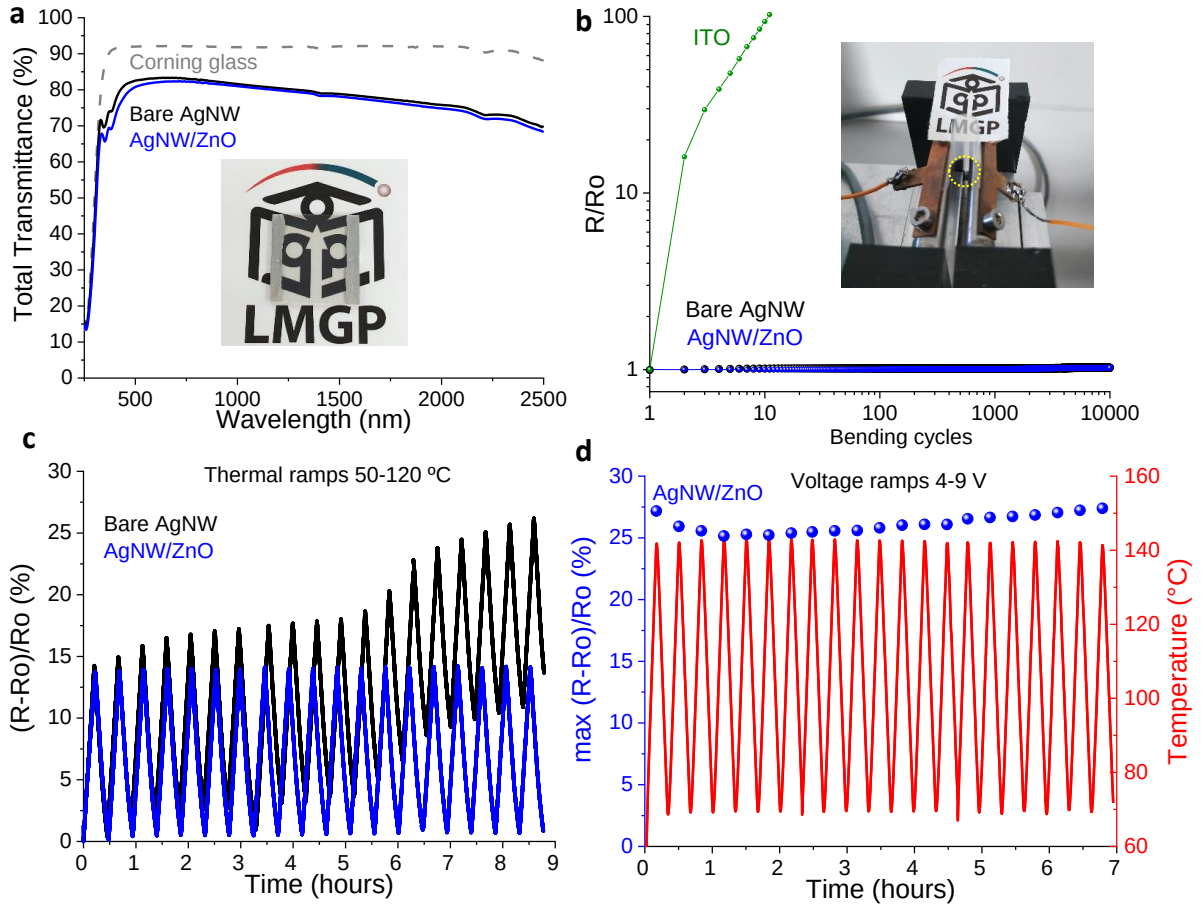

Figure 2. Physical properties and stability of AgNW-based TH; comparison between bare and 35 nm-ZnO coated networks. Bare AgNWs are represented in black and AgNW/ZnO in blue. (a) Total Transmittance in the UV-VIS-NIR spectrum, including the Corning glass substrate contribution, which is also plotted in grey dash line. (b) Relative electrical resistance change during 10000 bending cycles of 5 mm radius, compared to a commercial indium tin oxide (ITO, represented in green). (c) Relative electrical resistance change during 20 cycles of heating-cooling between 50 and 120 ºC, with a rate of ±5 ºC/min. (d) Maximum relative electrical resistance change (blue dots) in each cycle of 20 consecutive voltage ramps of ±0.5 V/min between 4 and 9 V, for ZnO coated AgNW networks. The red line corresponds to the Joule heating response during the voltage cycles.

2.3 Calibration of the lab-on-a-chip temperature

Once the fabrication and stability of the heating element were verified, the temperature of the liquid inside the microfluidic channels obtained for a particular bias applied to the TH had to be calibrated. The amount of heat released per unit of time is V^2/R (V is the bias while R is

the electrical resistance of the TH) and the power dissipated in the material is directly related to the achieved steady-state temperature, through a balance between the Joule heating and the heat losses.[13] These losses are due to: i) the thermal conduction directly to the substrate and then, indirectly, to the chip, ii) the convection to the surrounding air and iii) radiation emitted from the hot surfaces. This leads to a difference between the temperatures on the surface of the TH and the DNA solution inside the channels. The temperature of the device at different positions was then measured independently by using a thermocouple and IR imaging (Figure 3a). The type of electrical bias (ramp, plateau, and cycles) was also varied, and the experiments were repeated several times to verify the reproducibility with different AgNW/ZnO specimens and with 3 different SYBR Green I preparations. As schematically presented in **Figure 3**a, we measured and extrapolated the temperature in four different positions: a) T_1: surface temperature of TH by IR imaging, b) T_2: temperature of TH deduced by the electrical resistance measured by SMU (Source-Meter-Unit), c) T_3: channel temperature deduced by the fluorescence of SYBR Green inside the microchannel measured *in situ* by the microscope and d) T_4: temperature below the chip measured by conduction through a thermocouple (Pt100). For the IR imaging, the parameter of emissivity, ε, can influence significantly the measurement of T_1. Based on a recent study, we considered in the present work the following emissivity value for the AgNW network deposited on Corning glass: the value of ε=0.75.[37] For the calculation of T_2, based on the metallic behavior of the AgNW network, the linear dependence of the electrical resistance with the temperature is expressed by the following equation:

$$T_2 = T_0 + (R - R_0)/(\beta \cdot R_0)$$

where T_o is the initial-room temperature, R is the measured resistance at the temperature T_2, and R_0 is the initial resistance at room temperature. The temperature coefficient of electrical resistance, β, was derived as $2.5*10^{-3}$ K^{-1}, from the linear fitting of R versus T, as presented in Figure S1d.

To estimate T_3, we used the melting curve of a 448 bp-long DNA fragment, carried out in the presence of the fluorescent intercalant SybrGreen, performed in a qPCR CFX 96 Bio-Rad instrument (Figure S3). After background subtraction, fluorescence measurements were normalized to the value obtained at 25 °C (room temperature). The F(T)/F(25 °C) ratio is a decreasing function of temperature, whose reciprocal curve was used to compute the local temperature (see Methods section). In all recordings, when the local temperature extends up to DNA melting (80-81°C), the transition is clearly visible as a sharp decline in fluorescence

signal. This transition temperature is therefore unambiguously reached *in situ* during the recordings.

Figure 3b demonstrates the evolution of these temperatures during a voltage plateau of 3 V applied for 10 minutes (ON state) followed by a zero-bias step for a few minutes back the room temperature state (OFF state). During the OFF state, the electrical resistance was not measured thus, neither the temperature of the AgNW/ZnO was estimated. T_1 (IR) is represented in green, T_2 (from the AgNW resistance) is in blue, T_3 (channel, fluorescence) is in red while the T_4 (Pt100) is in gray. The temperatures follow the same evolution with a relatively constant difference and $T_1>T_2>T_3>T_4$. The IR temperature T_1, which is related to the radiation losses is close to the value of the temperature deduced from the electrical resistance of the specimen. As expected from the heat conduction losses, the temperature of the AgNW/ZnO network T_2 is higher than T_3 and T_4,. Due to the significant thickness of the glass substrate and plastic chip (1.1 mm in both cases) and the lower thermal conductivity of these materials compared to AgNWs, the difference between T_2 to T_4 can reach up to 20 °C in the explored temperature range. Similarly, the temperature inside the channel, T_3, deduced from the dye fluorescence, was between T_2 and T_4, and much closer to the TH temperature. This can be justified by the fact that the channels in the microchip are designed closer to the upper surface of the chip and the plastic has lower thermal conduction as well. In any case, the temperature gradient from T_1 to T_4 showed reproducible behaviour during constant applied bias, for instance, when repeating the same plateaus several times. This means that the electrical performance and the high stability of the TH are reliable not only for heating, but also to estimate the temperature inside the chip channels in a reproducible fashion. Additional experiments are provided in SI, concerning the comparison between IR imaging and temperature measurements by Pt100 thermocouple during a voltage ramp (Figure S4a), the comparison of temperatures measured in different positions of the thermocouple, i.e. under the chip or between the TH substrate and the chip (Figure S4b). The electrical and heating performance of the TH is very reproducible as demonstrated in Figure S4c, where 4 consecutive experiments (i to iv) of 3 V ON-OFF bias applied to the same AgNW/ZnO specimen are plotted.

In general, some of the potential issues tackled during the calibration experiments should be mentioned here, with the main one related to the chip's overheating. Reaching or passing 100 °C could lead sometimes to local melting of the channel and/or the evaporation of the DNA solution leading to the formation of air bubbles disturbing the fluorescent signal. This could also lead to the degradation of the biological sample, which is in any case very sensitive to long

air exposure, and high temperatures. Another issue could be the photo-bleaching of the fluorescent dye and in order to avoid it, the sample was not constantly exposed to the blue light but instead we used a shutter and recorded the fluorescent photos periodically, usually every 10 seconds.

2.4 *In situ* biological observations during homogeneous heating

Figure 3c demonstrates the evolution of the fluorescence of the SYBR Green I dye and the channel temperature, T_3, during 3 consecutive heating and cooling cycles between three voltage plateaus of 2.5, 3.7, and 4.5 V. A voltage ramp of 1 V/min was used between these values. At each cycle, the complete loss of fluorescence is obtained under a low applied bias of 4.5 V, reaching the melting of the DNA, (T_m) as indicated by the deduced channel temperature T_3 as well. These results prove the efficient and reproducible heating performance of the AgNW/ZnO based TH, as well as its low thermal inertia, which allows the channel to heat and cool down rapidly, with rates of 8.5 °C/min and -25 °C/min, respectively. Additional experiments of consecutive cycles are provided in Figure S4d. All the TH samples fabricated and used throughout our study were reusable and stable for more than 6 months.

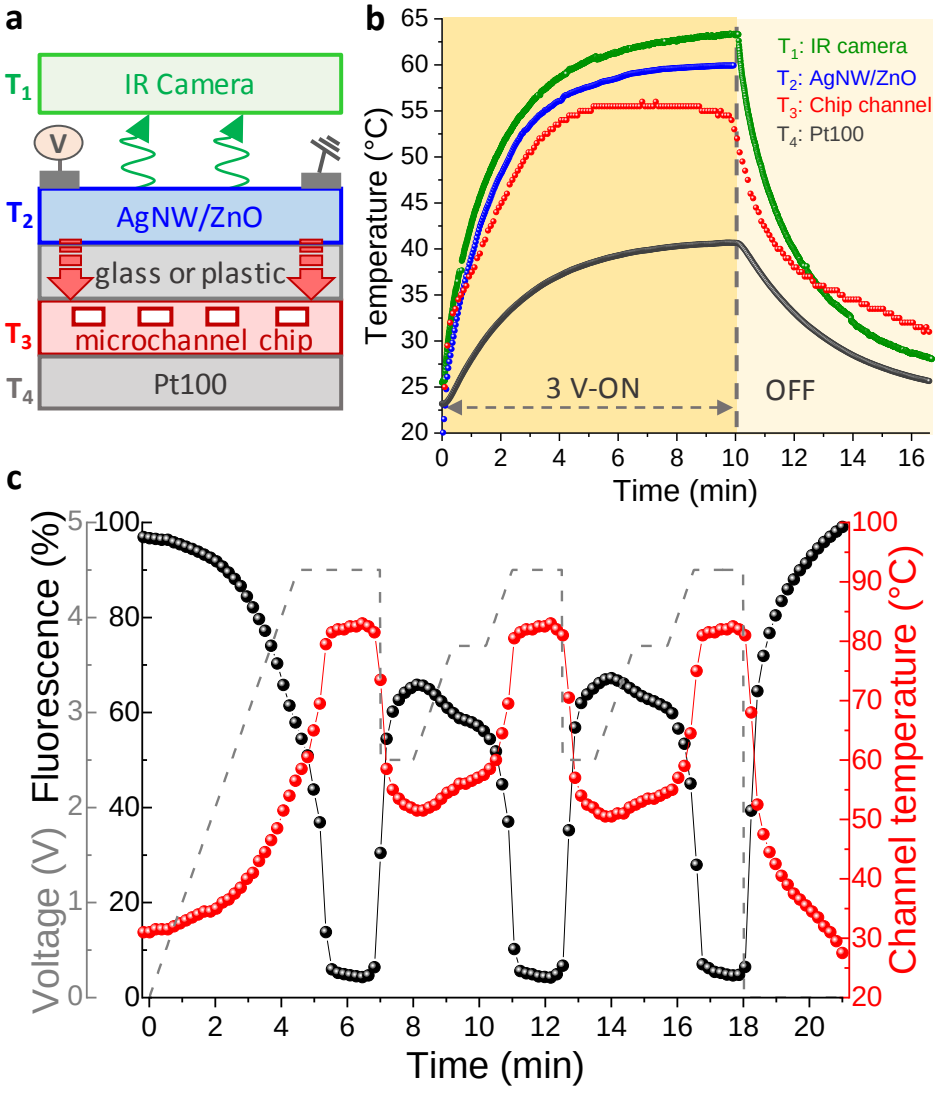

Figure 3. Temperature calibration of the lab-on-a-chip and *in situ* fluorescence measurements during voltage cycles applied to AgNW/ZnO based TH. (a) Schematic representation of the lab-on-a-chip cross-section. The layer thicknesses are not drawn at the same scale: the schema is simplified to highlight the different locations of temperature measurements. T_1 is measured by radiation-IR imaging (in green), T_2 is deduced from the electrical resistance of the AgNW-based TH (in blue), T_3 is deduced from the fluorescence of the dye inside the chip (in red) and T_4 is the temperature measured by conduction-thermocouple Pt100 (in gray). (b) Temperature versus time during a 3 V plateau applied for 10 minutes to AgNW/ZnO, followed by 0 V. (c) Normalized fluorescence of the SYBR Green I (in black dots) versus time measured *in situ* every 10 sec during 3 heating-cooling cycles with the deduced T_3 temperature inside the channel (red dots). The applied voltage (grey dash line) includes 3 plateaus, 2.5 and 3.7 V for 1 min and 4.5 V for 2.5 min initially and then 1.5 min. A ramp of 1 V/min is applied between the plateaus.

2.5 Fabrication and modelling of TH for localized heating

So far, we have demonstrated the pertinence of *in situ* observations of the fluorescence of the SYBR-Green I dye bound to dsDNA in solution inside one channel of a microfluidic chip and its evolution during heating-cooling cycles induced by a AgNW based TH. In this section, we present the development of a versatile TH for localized heating, in order to investigate the spatial or temporal distribution of the fluorescence either in different sections of a channel or in two separate channels simultaneously. For this, AgNW networks that contain regions of different network density, i.e. with different local electrical resistivity, were fabricated. Thus, these regions undergo a different level of Joule heating when a certain voltage is applied to the entire AgNW network. To achieve this, we have designed and fabricated 3D printed plastic masks. The low temperature, at which the networks are deposited, allows the use of such a low-cost, plastic masking technique. As represented schematically in **Figure 4**a, the masks were placed on the substrate after an initial deposition of nanowires, to block further deposition of nanowires in specific regions. All AgNW networks were finally coated with the same thickness of ZnO coating as mentioned above, for enhanced stability. Several types of patterns were developed during our studies; here we discuss the example of parallel bands, with sizes that fit the channels of the microfluidic chip. The chip channel width is 1 mm and the distance between the channels is 4.5 mm, thus we designed each band with a 7 mm width. During the spray deposition, we started by covering the whole substrate with nanowires. When the resistance, which is monitored *in situ* in a reference sample during the deposition of the nanowires, dropped below 80 Ω in the reference sample, we placed the mask (picture in Figure 4b-i) on top of the substrates and we continued the deposition until the reference sample reached a typical value of 10-15 Ω. The resulting network has regions with different network densities, as shown by the different optical contrast between them: the middle perpendicular band, which was masked, has fewer nanowires and thus it looks less opaque (picture in Figure 4b-ii). The adjacent/non-covered bands presented the typical *amd*, similar to the specimens discussed above. The resulted resistance, of the specific specimen used for the experiments presented below, was 22 Ω. Since the bands are in series and not in parallel, the electrical current crossing the AgNW network is supposed to be the same. This means that the region in the middle, which has a lower amount of deposited nanowires and thus higher local electrical resistivity, is hotter (I^2R). Furthermore, we have developed physical modelling by Comsol Multiphysics (the used parameters are provided in Methods section) to predict the electrical properties and thermal performance of Ag thin films. The films have bands of different electrical properties that

correspond to the local network density. This approximation allowed us to overcome the computational limits and simulate specimens of the same size as the experimental ones. Figure 4c and d provide the spatial distribution of the temperature obtained by modelling and IR imaging, respectively, for 5.3 V applied. The simulated electrical potential and surface current density distribution are provided in Figure S4e-f. The simulated values are in good agreement with the experimental ones, meaning that this approach can be used during the development of transparent heaters serving the specific needs of lab-on-a-chip devices.

2.5.1 *In situ* biological observations in a microfluidic chip during localized heating

The patterned AgNW based TH was integrated into two different configurations of the microfluidic chip channels and two types of experiments were performed. In the first case, we used a chip containing channels parallel to the long edge of the chip, as in the experiments presented so far, in order to investigate the heating of the biological sample at different temperatures in the same channel under the same voltage. The patterned TH was placed as shown in the picture in Figure 4e and the spatial distribution of the fluorescence of one channel was monitored *in situ* during a voltage plateau. A bias of 5.3 V was applied and the monitoring began after 9 minutes, when the T_m of the dsDNA and a steady-state regime for the TH were reached. The spatial distribution of the fluorescence was monitored with a scanning along the channel, with a 0.5 mm distance between two points of measurement. Normalized fluorescence and channel temperature (T_3) at each point inside the channel are plotted in Figure 4g. This temperature profile demonstrates clearly that there are three regions of different temperatures, which spatially correspond to the bands of different AgNW network densities.

In the second case, we used a different chip in which the channels were perpendicular to the long side of the chip, to investigate the evolution of the fluorescent dye simultaneously in two adjacent channels that are heated at different temperatures under the same applied bias to the TH. This time, the patterned TH was placed with the bands parallel to the microfluidic channels. The first channel is covered with the sparser AgNW middle band, while the second channel is exposed to the denser right band. More details about the chip dimensions are presented in the Methods section. A voltage ramp of 0.5 V/min was applied up to 6.5 V, to ensure that the T_m was reached. During this, the fluorescence of each channel was recorded consecutively *in situ* every 10 seconds. The results showed clearly a different heating for each channel. As shown in Figure 4h, channel 1, covered by the sparser band, reached higher temperature and in a faster

way, as expected given the different *amd* and thus local *R* value. Once the applied voltage was turned off and the TH started cooling down, the fluorescent signal of both channels recovered as well. However, back at room temperature, the average difference between the initial and final fluorescence, for three experiments performed consecutively, was +20% (channel 1) for the hotter channel and +5% for the colder one (channel 2). This increase in the fluorescence can be related to a local deformation of the plastic chip due to the high heating, mostly in the case of the hotter channel that reached 100 °C.

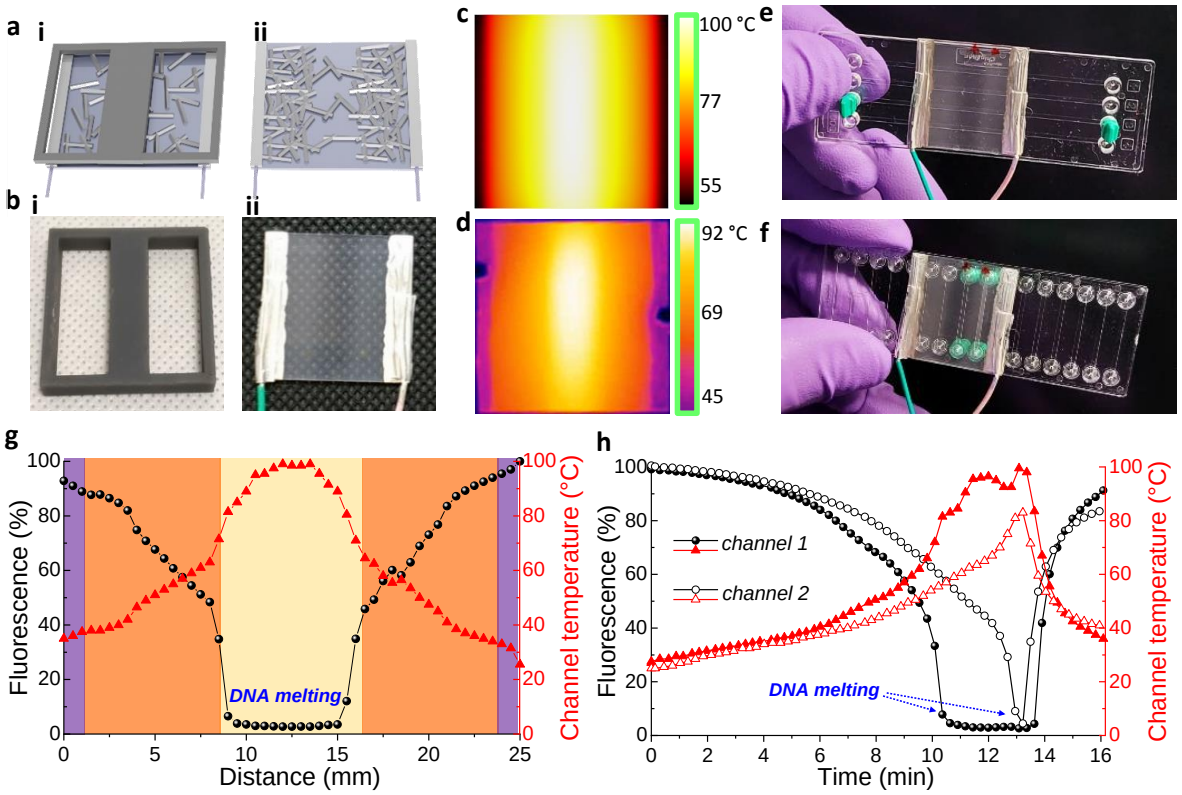

Figure 4. Development of AgNW/ZnO based TH for localized heating and *in situ* measurements of fluorescence spatial distribution in one channel and time evolution in two channels simultaneously. (a) Schematic representation of the 3D printed mask placed during the AgNW spray deposition (i), once the network resistance has decreased to less than 100 Ω. Thus, the final AgNW network (ii) has a lower nanowire density in the middle band. (b) Optical pictures of the plastic 3D-printed mask (i) and the TH after ZnO and contacts deposition (ii). The network density is lower in the middle as also shown by the optical contrast-transparency. (c) Surface temperature distribution by physical modeling of the TH at 5.3 V applied bias. (d) Surface temperature distribution of TH at 5.3 V during an applied voltage ramp. (e) Optical picture of the lab-on-a-chip configuration for *in situ* study of spatial fluorescence distribution

in one channel in lengthwise orientation chip. The TH has three parallel bands, the one in the middle with a lower AgNW density (associated with a larger resistance), and they are placed perpendicular to the channels. (f) Optical picture of the lab-on-a-chip configuration for *in situ* study of multiple channels fluorescence in crosswise orientation chip. The TH bands are placed parallel to the adjacent channels, which have a 4.5 mm distance between them, so that each of them heats homogeneously but at different temperatures. (g) Normalized fluorescence (black dots) measured *in situ* with a step of 0.5 mm inside a channel during a plateau of 5.3 V applied to the TH (e configuration). The deduced spatial distribution of the temperature is plotted as well (red triangles). (h) Normalized fluorescence (dots) measured for two channels *in situ* during a voltage ramp of 0.5 V/min until 6.5 V applied to the TH (f configuration) and the deduced temperature is plotted as well (triangles). Every 10 seconds the fluorescence was measured at each channel consecutively. The left channel (filled dots and triangles) was heated by the more resistive, middle band and reached faster the DNA melting point compared to the right channel (open dots and triangles).

3. Conclusions

In the present work, we demonstrated a proof-of-concept integration of transparent heaters (TH) based on AgNW networks into *in situ* biological studies in an optical microscope. AgNW were deposited and protected by a ZnO oxide layer, using open-air, low-temperature processes, compatible with large-scale production (spray coating and spatial atomic layer deposition, respectively). The fabricated TH are flexible and thus reusable, being easily placed and removed from microfluidic chips and remained stable after several months of use. In addition, selective heating can be achieved by easily patterning the TH thanks to conventional 3D printed plastic masks. Using AgNW/ZnO based TH, presenting a typical electrical sheet resistance of 10-15 Ω/sq and 2.5x2.5 cm^2 size, temperatures up to 100 °C could be reached inside the chip channels with less than 6.5 V applied bias, depending on the pattern of the AgNW network.

In situ biological observations were highly facilitated by the fabricated lightweight and low-energy-consumption transparent heating elements, exhibiting robustness and reproducibility. This is very important given the new challenges related to pandemic situations that require effective means for the detection of biological and viral species in a fast, reliable and low-cost way. The fluorescence of SYBR Green I dye, bound to dsDNA in solution inside the channels, was recorded during consecutive heating-cooling cycles. DNA denaturation-renaturation was

observed in every cycle, and the derived temperature inside the channels followed the same evolution as expected from the TH performance and physical modelling. Selective heating thanks to simply patterned TH was demonstrated both, by the spatial gradient of the temperature inside one channel and by the different temperatures inside two adjacent microchannels observed in parallel. The versatile AgNW-based TH reported in this study can be readily applicable to research studies and applications where localized heating and transparency are needed, for instance, to perform crystallization studies in microfluidic reactors, for cell culture and lab-on-a-chip systems or for transparent displays, among others.

4. Methods

4.1 AgNW synthesis and networks fabrication

AgNWs with an aspect ratio close to 100 (average diameter of 70 ± 10 nm and an average length of 8 ± 3 µm) were kindly provided from the research team of Jean-Pierre Simonato from CEA-LITEN in Grenoble, France, being produced as detailed in Mayousse et al.[38] The AgNWs were dispersed in methanol with an initial concentration of 3.9 g/L and diluted afterwards 30 times to obtain a concentration of 0.1 g/L. Spray deposition was performed with an airbrush of 0.4 mm nozzle size ("Infinity" by Harder & Steenbeck) and a nitrogen inlet of 1.4 bar pressure. The airbrush was fixed in a mechanical setup connected with a programmable automation controller. During deposition, the airbrush was moving along a regular and periodic array in X and Y directions, 7 cm above an aluminium plate set to 110 °C, for a direct evaporation of the solvent. The substrates used, Alkaline earth boroaluminosilicate glass (Corning® 1737, thickness 1.1 mm), were cut in squares of 25x25 mm^2, rinsed with acetone, sonicated for 15 min in isopropanol, rinsed with distilled water, and finally dried with N_2 gas. 0.1 mm thick flexible, transparent polyimide substrates of the same size, were used as well (Neopulim® kindly provided by Mitsubishi). To fabricate the patterned AgNW networks, masks made by a 3D printer with high temperature resin (version FLHTAM01 by Formlabs, Inc.) were placed on the top of the substrate during spray deposition.

4.2 Oxide coating

ZnO thin films were deposited with the atmospheric-pressure spatial atomic layer deposition (AP-SALD) home-made system of LMGP.[33,39] Diethylzinc (DEZ, $(C_2H_5)_2Zn$, Aldrich), and water vapor were used as precursors for zinc, and oxygen, respectively. The substrate

temperature was maintained at 200 °C. The gas injector was fixed at 150 µm from the substrate, which oscillated at 10 cm/s between different precursor channels to produce 100 ALD cycles, corresponding to 30±5 nm thick ZnO coating.

4.3 Microfluidic chip transparent heater set-up

Two types of Topas straight channel chips (purchased from microfluidic ChipShop®) were used throughout the experiments. The dimensions of both chips are 75.5 mm x 25.5 mm x 1.5 mm and the fluidic interface in order to fill the channel by pipetting has the shape of mini luer. The channel width and depth are 1 mm and 0.2 mm, respectively, and the distance between the channels is 4.5 mm. One chip has four channels of 58.5 mm length and lengthwise channel orientation, and the other sixteen channels of 18 mm length and crosswise channel orientation. Silver paste contacts (L-200N purchased from CDS Electronique) were manually deposited at two opposite sides of the AgNW/ZnO network and then thin, long copper wires were stuck to the silver paste and were connected to the power supply. For the demonstration of the lab-on-a-chip device, the AgNW/ZnO network on its polymeric substrate was attached with double coated adhesive tape (3M™ 9629PC) on top of the microfluidic chip.

4.4 Experimental characterizations

AgNWs and film surface morphology were analyzed by field emission gun-scanning electron microscopy (FEG-SEM Environmental FEI QUANTA 250 and SEM ZEISS-Gemini 300) and transmission electron microscopy (JEOL JEM-2010 microscope). ImageJ software was used to calculate the AgNW network density, expressed as the areal mass density *amd* (in mg/m^2), by a wire detection plug-in (Ridge detection), estimating the geometrical density in SEM images, following the protocol described somewhere else.[40] Optical properties were analyzed using a Lambda 950 spectrophotometer from Perkin Elmer in the 250–2500 nm range. The electrical, thermal, and mechanical properties of AgNW based transparent electrodes were investigated by experimental homemade set-up. For the thermal ramp tests, the samples were placed on top of a hotplate, whose temperature is controlled by temperature programmer/controller (Eurotherm) connected to a LabVIEW software. For the bending tests, the samples were placed between two jaws, whose position was moved using a motor, piloted by a LabVIEW. During the thermal ramps and the bending tests, a voltage of 0.1 V was applied by two-point probes and a source-measure-unit (SMU) (Keithley 2400) piloted by LabVIEW software as well, in

order to record the electrical resistance of the sample. The software allowed the recording of the temperature, voltage, current and resistance of the sample in real-time. The sourcemeter and the LabVIEW software were also used to control the voltage and measure the electrical resistance of the samples during the electrical tests and also for the heating of the microfluidic chip during the *in situ* optical microscope observations. The surface temperature spatial distribution of the specimens was measured by a FLIR T335 IR camera and by a resistance temperature detector (Pt100 RTD) embedded in a 120 µm thick PET layer. To monitor temperature *in situ*, SYBR Green I-DNA fluorescence in the microfluidic channels was observed with an Olympus IX71 inverted microscope equipped with a DP30DW camera, a 10x magnification objective and a 100 W Hg lamp. A motorized stage was used to switch channels during observations. The fluorescence was recorded and analyzed with Image Pro Plus 5 software.

4.5 Measurement of temperature inside the microfluidic channels

A pQE30 plasmid encoding *Dictyostelium discoideum* syntaxin 8 coding sequence (pQE30-Syn8) was used as a source of DNA.[41] A 448 bp-long DNA fragment containing Syn8 coding sequence was amplified with the following 5' and 3' primers (5' : TTTTTTCGCATCACCATCACCA; 3' : GCTTGGCTGCAGGTCGACCCGGG, 8 pmoles each), using BioRad Sso1 SYBR Green I qPCR mix (20 µL assay). qPCR was performed in a CFX-96 instrument (2 min 94°C denaturation, 20 cycles at 94°C (30 s), 50°C (30 s), 72°C (1 min). After amplification, a melting curve was acquired from 25°C to 95°C by 0.5°C steps. As a control, a sample without template DNA was prepared in the same manner. The signal obtained in the absence of sample (blank) was subtracted to calculate specific fluorescence. Specific fluorescence measurements were normalized to the value obtained at 25°C. The F(T)/F(25°C) ratio is a decreasing function of temperature, which can be adjusted with the following empirical equation:

$$\frac{F(T°C)}{F(25\,°C)}(\%) = a - \frac{bT + c + dTe^{\frac{T_m - T}{w}}}{1 + e^{\frac{T_m - T}{w}}}$$

in the range 35-95°C, using the following parameters : a = 148, b = 0.081 °C^{-1}, c=138, d=1.60 °C^{-1}, T_m=80.2 °C, w=0.82 °C. Above 81°C, the fluorescence signals of sample with and without DNA matches, indicating that the residual fluorescence is due to free SYBR Green I. In the

range 25-35°C, the fitting was extended using a cubic polynomial defined by its value of 100 at 25°C and the value and slope of F(T)/F(25°C) at 35°C :

$$\frac{F(T°C)}{F(25\ °C)}(\%) = 100 - a'(T-25) - b'(T-25)^2 - c'(T-25)^3$$

using the following parameters: a' = 0.3313 $°C^{-1}$, b' = 0 and c' = 4.224 10^{-3} $°C^{-3}$. A calibration curve relating the specific fluorescence ratio F(T)/F(25°C) as a function of T in the range 25-95°C was therefore obtained with a precision of 0.5°C. The reciprocal curve was used to deduce the local temperature from the F(T)/F(25°C) ratio. Practically, the blank signal was measured outside the microchannel containing SYBR Green I-DNA sample and the initial specific fluorescence was recorded before heating at room temperature F(25°C). The specific fluorescence ratio F(T)/F(25°C) was compared to the calibration curve to compute the local temperature with a precision of 0.5°C.

4.6 Modeling

Physical simulations of homogeneous and masked AgNW networks were performed using Comsol Multiphysics® version 5.2 and the AC/DC Module. The software is based on finite element analysis and the physics of "Electric Currents, Shell" and "Heat transfer in solids" were used, coupling both electrical and thermal models and thus calculating the spatial distributions of the electric potential, current density, and surface temperature. A thin Ag film on top of Corning glass of 3 nm was simulated to represent the AgNW networks, as described in the simulations performed in our previous work.[16] Although AgNW constitute nanomaterials for which sizes can be of the same order of magnitude of electrons mean free path, we considered for the sake of simplicity through Comsol simulations heat transfer modeling within a continuous medium. The thin film has three parallel bands of different electrical properties, corresponding to the experimental patterned AgNW networks, fabricated with the help of the 3D printed masks. In the case of less dense band in the middle, the sheet resistance was set to 80 Ω/sq, while the rest of the specimen was set to 10 Ω/sq. The size of the simulated specimens was the same as the experimentally fabricated ones (25x25 mm^2) as well as the glass substrate size (25x25x1.1 mm^3). A work plane was added, where rectangular contacts with a width of 1.5 mm were added on the left and the right sides with the appropriate electric boundary conditions. To perform thermal simulations, three main mechanisms of heat losses were taken into account: convection, conduction, and radiation. In the model, the two layers were not physically

separated so the conduction between them is considered ideal and any external conduction losses were neglected (for instance the conduction losses through the connecting wires were not taken into account). The emissivity of Corning glass was considered for the radiation losses and the value of 0.75 was considered for the Ag film, same as the AgNW network value set for the IR imaging in the experiments. Concerning the convection losses, a heat transfer coefficient of h= 10 W/(m^2.K) was applied for the glass substrate, h= 50 W/(m^2.K) for the silver layer and h= 40 W/(m^2.K) for the less dense/conductive band.

Supporting Information

Supporting Information is available from the Wiley Online Library.

Acknowledgements

This study was performed within the framework of the Centre of Excellence of Multifunctional Architectured Materials (CEMAM) n°ANR-10-LABX-44-01. Agence Nationale de la Recherche (ANR) is acknowledged for financial support under contracts ANR-18-CE09-0040 (MEANING), ANR-18-CE09-0036 (PANASSE) and ANR-15-IDEX-02 (Eco-SESA). The authors would like to thank Laetitia Rapenne for her contribution to the nanowire characterization by TEM, Cesar Arturo Masse de la Huerta for his contribution to the 3D-printing of the masks and Jean-Pierre Simonato for fruitful discussions.

References

[1] V. Miralles, A. Huerre, F. Malloggi, M.-C. Jullien, *Diagnostics* **2013**, *3*, 33.
[2] J. Chen, Z. Luo, L. Li, J. He, L. Li, J. Zhu, P. Wu, L. He, *Lab Chip* **2018**, *18*, 412.
[3] C. D. Ahrberg, A. Manz, B. G. Chung, *Lab Chip* **2016**, *16*, 3866.
[4] W. Zhang, N. Li, D. Koga, Y. Zhang, H. Zeng, H. Nakajima, J.-M. Lin, K. Uchiyama, *Anal. Chem.* **2018**, *90*, 5329.
[5] K. H. Chung, Y. H. Choi, H. K. Choi, J. T. Kim, Y.-J. Yu, J. S. Choi, D.-H. Youn, C.-G. Choi, in *IEEE SENSORS 2014 Proceedings*, IEEE, Valencia, Spain, **2014**, pp. 1006–1009.
[6] S.-R. Joung, J. Kim, Y. J. Choi, C. J. Kang, Y.-S. Kim, in *2007 2nd IEEE International Conference on Nano/Micro Engineered and Molecular Systems*, IEEE, Bangkok, **2007**, pp. 691–694.
[7] K. Sun, A. Yamaguchi, Y. Ishida, S. Matsuo, H. Misawa, *Sensors and Actuators B: Chemical* **2002**, *84*, 283.
[8] T. Sannicolo, M. Lagrange, A. Cabos, C. Celle, J.-P. Simonato, D. Bellet, *Small* **2016**, *12*, 6052.

[9] W. Li, H. Zhang, S. Shi, J. Xu, X. Qin, Q. He, K. Yang, W. Dai, G. Liu, Q. Zhou, H. Yu, S. R. P. Silva, M. Fahlman, *J. Mater. Chem. C* **2020**, *8*, 4636.
[10] M.-R. Azani, A. Hassanpour, T. Torres, *Advanced Energy Materials* **2020**, *10*, 2002536.
[11] X. Lu, Y. Zhang, Z. Zheng, *Adv. Electron. Mater.* **2021**, 2001121.
[12] D. Li, W.-Y. Lai, Y.-Z. Zhang, W. Huang, *Advanced Materials* **2018**, *30*, 1704738.
[13] D. T. Papanastasiou, A. Schultheiss, D. Muñoz- Rojas, C. Celle, A. Carella, J.-P. Simonato, D. Bellet, *Advanced Functional Materials* **2020**, *30*, 1910225.
[14] O. Ergun, S. Coskun, Y. Yusufoglu, H. E. Unalan, *Nanotechnology* **2016**, *27*, 445708.
[15] Q. Huang, W. Shen, X. Fang, G. Chen, J. Guo, W. Xu, R. Tan, W. Song, *RSC Advances* **2015**, *5*, 45836.
[16] D. T. Papanastasiou, N. Charvin, J. Resende, V. H. Nguyen, A. Sekkat, D. Muñoz-Rojas, C. Jiménez, L. Flandin, D. Bellet, *Nanotechnology* **2021**, *32*, 445702.
[17] N. Charvin, J. Resende, D. T. Papanastasiou, D. Muñoz-Rojas, C. Jiménez, A. Nourdine, D. Bellet, L. Flandin, *Nanoscale Adv.* **2021**, *3*, 675.
[18] T. Sannicolo, N. Charvin, L. Flandin, S. Kraus, D. T. Papanastasiou, C. Celle, J.-P. Simonato, D. Muñoz-Rojas, C. Jiménez, D. Bellet, *ACS Nano* **2018**, *12*, 4648.
[19] J. J. Patil, W. H. Chae, A. Trebach, K. Carter, E. Lee, T. Sannicolo, J. C. Grossman, *Adv. Mater.* **2020**, 2004356.
[20] J. Bang, S. Coskun, K. R. Pyun, D. Doganay, S. Tunca, S. Koylan, D. Kim, H. E. Unalan, S. H. Ko, *Applied Materials Today* **2021**, *22*, 100909.
[21] A. Khan, V. H. Nguyen, D. Muñoz-Rojas, S. Aghazadehchors, C. Jiménez, N. D. Nguyen, D. Bellet, *ACS Applied Materials & Interfaces* **2018**, *10*, 19208.
[22] A. Sekkat, V. H. Nguyen, C. A. Masse de La Huerta, L. Rapenne, D. Bellet, A. Kaminski-Cachopo, G. Chichignoud, D. Muñoz-Rojas, *Commun Mater* **2021**, *2*, 78.
[23] L. Bardet, D. T. Papanastasiou, C. Crivello, M. Akbari, J. Resende, A. Sekkat, C. Sanchez-Velasquez, L. Rapenne, C. Jiménez, D. Muñoz-Rojas, A. Denneulin, D. Bellet, *Nanomaterials* **2021**, *11*, 2785.
[24] C. A. M. de la Huerta, V. H. Nguyen, A. Sekkat, C. Crivello, F. Toldra- Reig, P. B. Veiga, S. Quessada, C. Jimenez, D. Muñoz- Rojas, *Advanced Materials Technologies* **2020**, *5*, 2000657.
[25] D. Muñoz-Rojas, T. Maindron, A. Esteve, F. Piallat, J. C. S. Kools, J.-M. Decams, *Materials Today Chemistry* **2019**, *12*, 96.
[26] D. Li, X. Liu, X. Chen, W. Lai, W. Huang, *Adv. Mater. Technol.* **2019**, *4*, 1900196.
[27] D. Li, W. Lai, F. Feng, W. Huang, *Adv. Mater. Interfaces* **2021**, *8*, 2100548.
[28] D. Nieto, P. McGlynn, M. de la Fuente, R. Lopez-Lopez, G. M. O'connor, *Colloids and Surfaces B: Biointerfaces* **2017**, *154*, 263.
[29] Z. Lei, D. Xie, M. K. Mbogba, Z. Chen, C. Tian, L. Xu, G. Zhao, *Lab Chip* **2019**, *19*, 1929.
[30] L. J. Romasanta, P. Schäfer, J. Leng, *Scientific Reports* **2018**, *8*, 16227.
[31] L. Leroy, R. Bombera, E. Engel, R. Calemczuk, L. Laplatine, D. R. Baganizi, P. N. Marche, Y. Roupioz, T. Livache, *Lab Chip* **2014**, *14*, 1987.
[32] J. Resende, D. T. Papanastasiou, D. C. Moritz, N. Fontanals, C. Jiménez, D. Muñoz-Rojas, D. Bellet, *ACS Appl. Nano Mater.* **2022**, acsanm.1c03821.
[33] V. H. Nguyen, J. Resende, C. Jiménez, J.-L. Deschanvres, P. Carroy, D. Muñoz, D. Bellet, D. Muñoz-Rojas, *Journal of Renewable and Sustainable Energy* **2017**, *9*, 021203.
[34] R. D. Raninga, R. A. Jagt, S. Béchu, T. N. Huq, W. Li, M. Nikolka, Y.-H. Lin, M. Sun, Z. Li, W. Li, M. Bouttemy, M. Frégnaux, H. J. Snaith, P. Schulz, J. L. MacManus-Driscoll, R. L. Z. Hoye, *Nano Energy* **2020**, *75*, 104946.
[35] C. Schneeberger, P. Speiser, F. Kury, R. Zeillinger, *Genome Research* **1995**, *4*, 234.

[36] G. Giusti, V. Consonni, E. Puyoo, D. Bellet, *ACS Applied Materials & Interfaces* **2014**, *6*, 14096.
[37] S. Hanauer, C. Celle, C. Crivello, H. Szambolics, D. Muñoz-Rojas, D. Bellet, J.-P. Simonato, *ACS Appl. Mater. Interfaces* **2021**, acsami.1c02689.
[38] C. Mayousse, C. Celle, E. Moreau, J.-F. Mainguet, A. Carella, J.-P. Simonato, *Nanotechnology* **2013**, *24*, 215501.
[39] D. Muñoz-Rojas, V. H. Nguyen, C. Masse de la Huerta, S. Aghazadehchors, C. Jiménez, D. Bellet, *Comptes Rendus Physique* **2017**, *18*, 391.
[40] V. H. Nguyen, J. Resende, D. T. Papanastasiou, N. Fontanals, C. Jiménez, D. Muñoz-Rojas, D. Bellet, *Nanoscale* **2019**, *11*, 12097.
[41] A. Bogdanovic, N. Bennett, S. Kieffer, M. Louwagie, T. Morio, J. Garin, M. Satre, F. Bruckert, *Biochemical Journal* **2002**, *368*, 29.

Table of Contents

Lightweight, flexible and highly stable transparent heaters based on silver nanowire networks, are integrated in lab-on-a-chip for *in situ* monitoring of biological processes. Localized heating using a single transparent heater and applied bias, is demonstrated inside one microchannel or for adjacent microchannels of the same chip heating at different temperatures.

D. T. Papanastasiou, A. Sekkat, V. H. Nguyen, C. Jiménez, D. Muñoz-Rojas, F. Bruckert*, D. Bellet*

Stable flexible transparent electrodes for localized heating of lab-on-a-chip devices

ToC Figure